



HAL
open science

Influence of particle size distribution on carbonbased flowable electrode viscosity and desalination efficiency in flow electrode capacitive deionization

Myriam Tauk, Mikhael Bechelany, Serge Lagerge, Philippe Sostat, Roland Habchi, Marc Cretin, Francois Zaviska

► To cite this version:

Myriam Tauk, Mikhael Bechelany, Serge Lagerge, Philippe Sostat, Roland Habchi, et al.. Influence of particle size distribution on carbonbased flowable electrode viscosity and desalination efficiency in flow electrode capacitive deionization. Separation and Purification Technology, In press, 10.1016/j.seppur.2022.122666 . hal-03860816

HAL Id: hal-03860816

<https://hal.umontpellier.fr/hal-03860816v1>

Submitted on 18 Nov 2022

HAL is a multi-disciplinary open access archive for the deposit and dissemination of scientific research documents, whether they are published or not. The documents may come from teaching and research institutions in France or abroad, or from public or private research centers.

L'archive ouverte pluridisciplinaire **HAL**, est destinée au dépôt et à la diffusion de documents scientifiques de niveau recherche, publiés ou non, émanant des établissements d'enseignement et de recherche français ou étrangers, des laboratoires publics ou privés.

1 Influence of particle size distribution on carbon- 2 based flowable electrode viscosity and 3 desalination efficiency in flow electrode 4 capacitive deionization.

5 Myriam Tauk, Mikhael Bechelany*, Serge Lagerge, Philippe Sostat, Roland Habchi, Marc Cretin
6 and Francois Zaviska*

7 Institut Européen des Membranes, IEM, UMR-5635, University of Montpellier, ENSCM, CNRS, Place
8 Eugène Bataillon, CEDEX 5, 34095 Montpellier, France;

9 myriam.tauk@umontpellier.fr (MT); mikhael.bechelany@umontpellier.fr (MB);
10 serge.lagerge@umontpellier.fr (SL); philippe.sostat@umontpellier.fr (PS); rhabchi@ul.edu.lb (RH);
11 marc.cretin@umontpellier.fr (MC); francois.zaviska@umontpellier.fr (FZ)

12 * Correspondance: marc.cretin@umontpellier.fr (MC), mikhael.bechelany@umontpellier.fr (MB),
13 francois.zaviska@umontpellier.fr (FZ)
14

15 Abstract

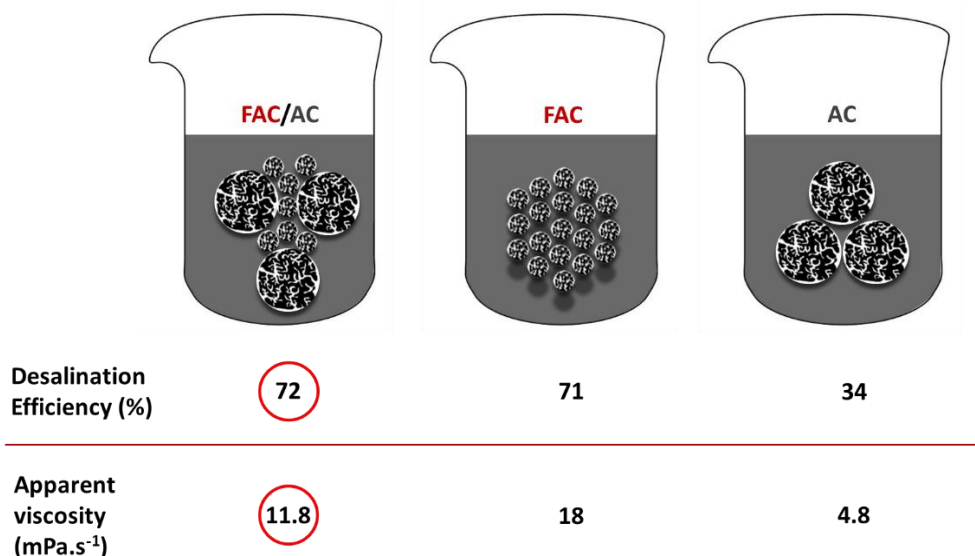
16 Flow-electrode capacitive deionization (FCDI) is a potential energy-efficient electrochemical
17 water desalination technology that combines ion-exchange membranes and flowable
18 electrodes (FE). The performance of activated carbon (AC)-based FEs in FCDI systems is
19 influenced by various factors, including particle size. Here, particle size commercial AC was
20 reduced by dry ball milling to produce FEs for FCDI. Physical analysis by scanning electron
21 microscopy and particle size analyzer confirmed the particle size reduction after dry ball milling.
22 Then, the effect of particle size distribution on the rheological behavior and desalination
23 performances of AC-based FEs was investigated by desalination performance indicators, such
24 as desalination efficiency, average salt adsorption rate and charge efficiency. FE samples
25 were prepared using different mixtures of fine-size range (0.65-0.92 μm ; fine AC, FAC) and
26 large-size range (1.5-2.3 μm ; AC) particles. The AC to FAC particle ratio influenced the
27 rheological properties of AC-based FEs in FCDI. Bimodal mixtures with 75% of FAC and 25%
28 of AC (0.75:0.25 FAC:AC) particles displayed the highest desalination efficiency compared
29 with pure AC and pure FAC FEs (72% *versus* 34% and 71%, respectively). Moreover, in our
30 FCDI set-up, 0.75:0.25 FAC:AC bimodal mixtures showed better flowing properties than the
31 pure FAC FEs, characterized by high viscosity.

32

33 **Keywords:** Flow electrode capacitive deionization, activated carbon flow electrode, particle size
34 distributions, rheology, stability and desalination.

35

36 **Graphical abstract**



37

38

39 **1. Introduction**

40 Capacitive deionization (CDI) is used to eliminate charged species from water with various
 41 applications, such as brackish and sea water desalination,^{1,2} water softening,³ and wastewater
 42 remediation.⁴ CDI is an energy-efficient, cost-effective, and ecofriendly technology.⁵ The first
 43 and most widely-used CDI set-up requires two porous carbon electrodes separated by a
 44 spacer through which water flows perpendicularly to the applied electric field.⁵ In membrane
 45 CDI (MCDI), a key variation of the basic CDI set-up⁶, the feed water flows between an anion
 46 exchange membrane at the anode and a cation exchange membrane at the cathode.⁷ The
 47 membrane main role is to reduce co-ion adsorption. This improves the charge efficiency and
 48 can increase the charge storage in the electrode porous structure.⁸ In the last decade, a new
 49 MCDI-based approach was developed to introduce carbon-based flowable electrodes.⁹ The
 50 basis of this technology, called flow-electrode CDI (FCDI), is similar to that of electrochemical
 51 flow capacitors¹⁰. The process is based on electrical double layers that are formed on
 52 interfaces between porous activated carbon (AC)-based electrodes and an electrolyte (e.g.
 53 NaCl solution).¹¹ Ions are adsorbed and stored in the electrical double layers when a cell
 54 voltage in the range of 1–1.2 V is applied to the cell¹². FCDI has three major advantages
 55 compared with other CDI systems. First, the continuous desalination of the feed water flowing
 56 through a single cell does not require an in situ discharge step for regenerating the ion-
 57 saturated AC-based electrodes, which is done in a separate process. This allows the easy
 58 scaling-up of FCDI¹³. Second, the continuous inflow of uncharged carbon particles into the
 59 charging cell increases the capacitance, which is needed for desalination, above that of static-
 60 electrode CDI systems.¹⁴ This offers more flexibility because the desalination rate and kinetics
 61 can be easily controlled by adjusting the saline solution, flow electrode retention time, and the
 62 applied current charge. Third, in AC-based flowable electrodes, pores are more exposed and
 63 easily accessible for ion adsorption.

64 The choice of electrode material is a crucial factor in CDI system performance. The ideal CDI
 65 electrode material should meet the following criteria: 1) large specific surface area, high ion

66 adsorption sites; 2) high conductivity and ion mobility; 3) hydrophilicity to ensure full contact
67 between the electrode porous structure and water; 4) electrochemical stability at different pH
68 and voltages to ensure the system reliability and sustainability; 5) easily shapeable in function
69 of the design requirements and economically feasible (i.e. availability, cost, and recyclability)
70 for industrial development. Carbon-based materials are mostly used in this field because they
71 meet these requirements. Moreover, to improve the properties of the carbon-based materials
72 used as CDI electrodes, many methods have been tested and many carbon forms have been
73 exploited, for instance AC, AC fibers, carbon aerogels, AC cloths,^{15,16} carbon nanotubes,¹⁷
74 graphene,¹⁸ carbon nanofibers,¹⁹ carbon sheet²⁰.

75 Porous AC, a cheap, easily available and reusable material, is widely used to prepare flowable
76 electrodes for FCDI.²¹ The electrochemical performance of AC-based flowable electrodes is
77 influenced by several parameters, including mass loading, particle size and morphology,
78 specific surface area, surface charge, viscosity, and hydrophilicity.²² However, they display low
79 wettability, pore inaccessibility for ions, and low conductivity. Therefore, to improve its features
80 and overcome some of its limitations, AC can undergo physical or chemical treatments. For
81 instance, pores can be expanded using physical treatments, such as thermal modification
82 using inert gases (e.g. N₂, Ar, CO₂).²³ Surface area can be improved by exposure to KOH or
83 NaOH followed by thermal treatment.²⁴ Much research has been done on hierarchical porous
84 carbons with interconnected micro-mesopores for increasing ion adsorption.²⁵ Recent studies
85 have investigated the particle size effect on the desalination performance of AC-based
86 electrodes in CDI.²⁶ Cohen *et al.* combined dilute slurry electrodes and dense fluidized bed
87 electrodes for better electric conductivity and lower resistance.²⁷ Zhang *et al.* found that AC-
88 based electrodes with different particle sizes provide different CDI performances. Particularly,
89 a mixture of large and small particles gave the best desalination performance in CDI.²⁶
90 However, the effect of particle size distribution on the viscosity and desalination performance
91 of carbon slurry electrodes in FCDI has not been investigated yet. In a previous study, we
92 found that reducing AC particle size in flowable electrodes can double the desalination rate in
93 FCDI.²⁸ This was attributed to the enhanced connectivity between particles that increases
94 charge transport and storage, thus improving conductivity through the AC percolating network.
95 Moreover, in AC-based electrodes with finer particles, obtained by grinding, pores were more
96 exposed, leading to faster ionic diffusion.²⁸ However, viscosity was increased upon particle
97 size reduction. As the flowable electrode must flow along a narrow channel in the FCDI set-
98 up, its rheological features are a crucial factor for limiting pressure drops and ensuring the
99 absence of clogging. Indeed, the higher viscosity of the flowable electrode with fine AC
100 particles, compared with normal AC particles, led to pumping and flowing difficulties inside the
101 FCDI system. Therefore, in the present study, we wanted to decrease the viscosity of AC-
102 based flowable electrodes, while maintaining the good desalination performance obtained with
103 fine AC particles. To this aim, we mixed two AC particle size ranges to produce flowable
104 electrodes for FCDI. We prepared bimodal slurries with different ratios of fine AC (FAC) to AC
105 particles with the same carbon loading (10%) and characterized their rheological properties
106 and desalination performance to find the best compromise between these parameters.

107 Our AC modification strategy for desalination improvement in FCDI is very simple, compared
108 with the complex physical and chemical AC modifications that have been recently used in CDI.
109 This is important, especially due to the major improvements in FCDI desalination efficiency

110 and viscosity reduction observed with these bimodal flowable electrodes compared with pure
111 AC and FAC flowable electrodes.

112

113 2. Experimental

114 2.1. Material preparation

115 Commercial AC (Darco; CAS no: 7440-44-0) and sodium chloride (NaCl, CAS no: 7647-14-5,
116 MW 58.44 g mol⁻¹, 99%) were purchased from Sigma Aldrich. Cationic and anionic exchange
117 membranes were purchased from Membranes International Inc. (Ringwood, New Jersey,
118 USA). Deionized water (18 MΩ cm⁻²) was prepared using a purification system.

119 AC powder was dry ball-milled using 50-mm diameter balls (350 rpm rotation speed) at room
120 temperature for 90 minutes to obtain finer particles (

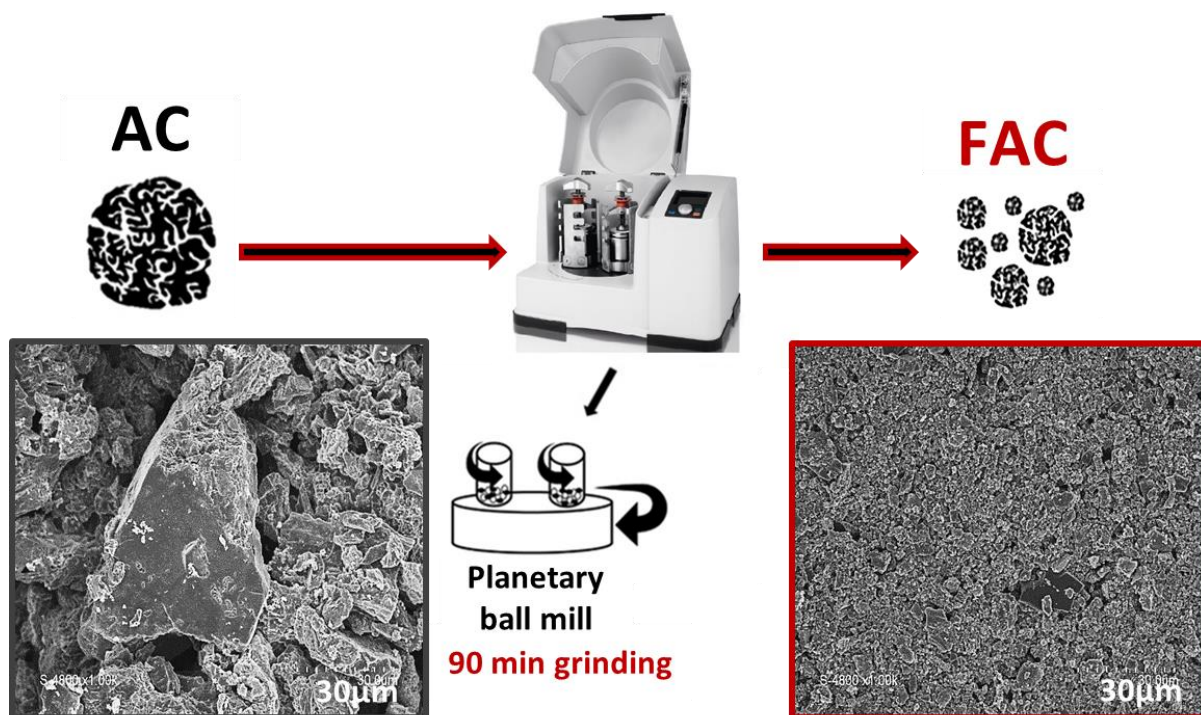
FE (10 % wt)	AC (% wt)	FAC (% wt)	[NaCl] (g/L) (V=70 mL)	
FE1	10	0	1	124
FE2	8	2	1	125
FE3	5	5	1	126
FE4	2.5	7.5	1	127
FE5	0	10	1	128

)**Erreur ! Source du renvoi introuvable.**²⁸ Ball-milled AC, called fine particle AC (FAC), and pristine AC with different particle size ranges (0.3-0.6 μm and 0.8-1.6 μm, respectively) were used for this study.

129 AC suspensions, used as flowable
130 electrodes, were prepared by mixing the desired amounts of AC and FAC (10% wt as total
131 weight percentage in each electrode) in 1 g/L NaCl solution (**Erreur ! Source du renvoi
132 introuvable.**). Two different packing characteristics were chosen; i) monomodal distribution,
133 where slurry electrodes contained only one particle size range (AC or FAC), and ii) bimodal
134 distribution where slurry electrodes were mixtures of AC and FAC at different ratios. Then, the
135 mixtures were sonicated for 2 h and stirred for 1 h to obtain a uniform particle distribution in
136 suspension. The slurry electrode in a beaker was continuously stirred and was fed into the cell
throughout the FCDI experiments (repeated three times for each sample).

137

138



139
140 **Figure 1:** Planetary dry ball milling of activated carbon (AC) into fine activated carbon (FAC).

141 **Table 1:** Composition of the flowable electrodes (FE) used in this study

FE (10 % wt)	AC (% wt)	FAC (% wt)	[NaCl] (g/L) (V=70 ml)
FE1	10	0	1
FE2	8	2	1
FE3	5	5	1
FE4	2.5	7.5	1
FE5	0	10	1

148

149 **2.2. AC Material Characterization**

150 For all sample characterizations, carbon suspensions prepared in 1 g/L NaCl solution
 151 (experimental conditions) were used. Our previous study included a detailed physical
 152 characterization of AC and FAC (after grinding) samples²⁸. AC and FAC particle size
 153 distribution and their zeta potentials were measured by dynamic light scattering using a
 154 Litesizer 500 particle size analyzer (Anton Paar, France). The particle structure was analyzed
 155 by scanning electron microscopy (SEM) (SEM, Hitachi S4800, Tokyo, Japan), and the atomic
 156 composition (chemical moieties) of the material was studied before and after ball milling
 157 (analyzed surface area = 300 x 700 µm) by X-ray photonelectron spectroscopy (XPS)
 158 (Spectrometre XPS/UPS KRATOS AXIS Ultra DLD). The surface area was measured using
 159 N₂ adsorption/desorption at 77 K. The specific surface area was calculated using the Brunauer-
 160 Emmett-Teller method (Micromeritics 2020 ASAP, Merignac France). The total pore volume
 161 (V_t) was calculated from the amount of N₂ adsorbed at 0.99 relative pressure (P/P₀). The

162 mesopore volume (V_{meso}) was calculated with the Barrett-Joyner-Halenda model. The dynamic
163 viscosity of the different carbon suspensions (flow electrodes) was measured using a Paar
164 Physica UDS 200 Rheometer, a concentric cylinder adapted for heterogeneous solutions or
165 water suspensions, as a function of the shear rate at 25 °C. Dynamic viscosity describes the
166 resistance of a liquid solution to flow, whereas the shear rate is the deformation speed of the
167 suspension under an applied force. The physical stability or sedimentation rate of the different
168 AC slurries over time was measured with a Formulaction TURBISCAN® in which static multiple
169 light scattering is used to monitor particle migration in liquids. A measurement head with two
170 detectors moves along the cell height to measure the transmission (T) and backscattering (BS)
171 signals that are related to particle size and concentration in the sample. The changes over time
172 are a sign of destabilization that is quantified using the TURBISCAN® stability index (TSI).
173 Each experiment was repeated three times for each electrode type. The electrochemical
174 properties of AC and FAC were tested by cyclic voltammetry (CV) method. CV tests were
175 performed using Orignalys OrigaStat OGS080 potentiostat and 3 electrodes system with a 5
176 mm carbon glass rotating disk electrode (RDE) as working electrode while a platinum mesh
177 and a saturated 3 M KCl, Ag/AgCl electrode served as counter and reference electrodes
178 respectively. 10% wt. activated carbon suspensions were prepared, 100 μl were deposited on
179 the surface of the RDE then dried at 80°C before adding one drop of nafion ink to hold the
180 material on the electrode. Voltammetry measurements were performed at a -0.2 V-0.4 V vs ref
181 operating potential window in 5 g/L NaCl solution as electrolyte. The electrical double layer
182 capacitance (EDLC) was determined using cyclic voltammetry cycles at 0.02 V. s^{-1} scan rate.

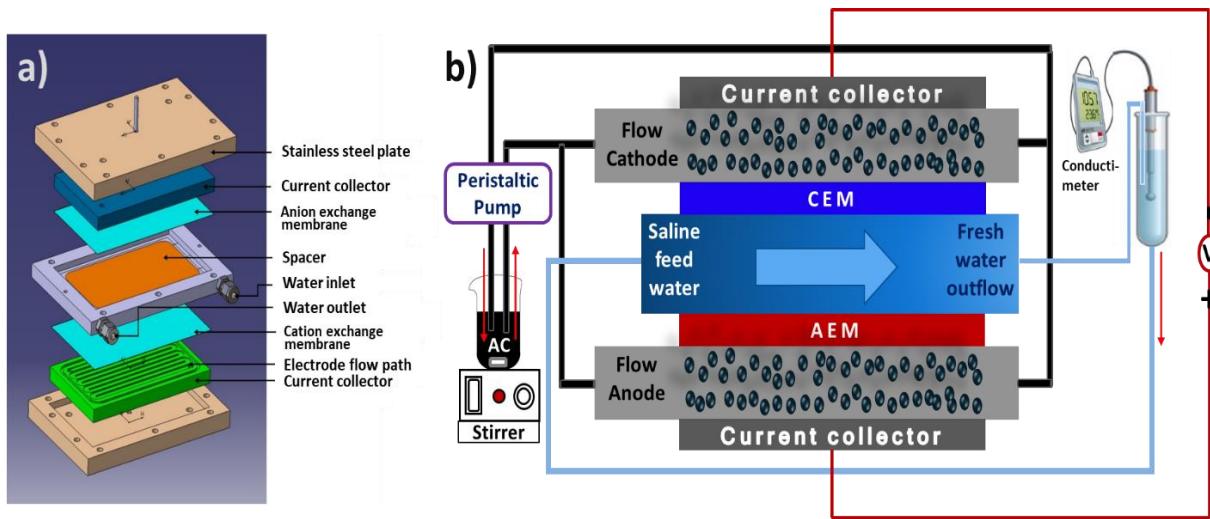
183

184 2.3. FCDI experiments

185 Figure 2 shows the FCDI experimental set-up and its operating principle. The system was
186 composed of a homemade FCDI cell, a potentiostat (Orignalys Electrochem, OrigaFlex), a
187 conducti-meter (HANNA Instruments) to monitor the saline solution conductivity during the
188 desalination experiment, and two beakers (one for the flowable electrode and the other for the
189 saline solution) with two peristaltic pumps to recirculate both solutions through the
190 electrochemical cell. Experiments were performed in a closed loop reactor at 1V constant
191 voltage, using 5g/L NaCl as feed solution (FS), and lasted 30 min. The FCDI cell (**Erreur !
192 Source du renvoi introuvable.**(a)), specifically designed for these experiments, was
193 composed of two current collectors (0.9mm depth, 8.5 cm width, and 14.5 cm length) with two
194 channels each as flow electrode inflow and outflow of 7.8 cm depth, two ion exchange
195 membranes (IEM) of 142 cm^2 effective area, a spacer (0.9 mm thick), two stainless steel plates,
196 and nails to hold all parts together.

197 The electrical field created inside the FCDI cell drives ions present in the FS (5 g/L NaCl)
198 through a spacer, sandwiched between two IEM, to be electrostatically attracted to the charged
199 flowable electrodes that circulate through the flow paths carved on the current collectors, as
200 shown in **Erreur ! Source du renvoi introuvable.**(a). When the flowable electrodes exit the
201 channels, they are fed back into the reservoir, stirred, and then re-circulated inside the cell.
202 The resulting current at the electrodes was monitored throughout the experiment by
203 chronoamperometry. The FS and flowable electrodes were flowing at a constant flow rate of 3
204 $\text{ml}\cdot\text{min}^{-1}$ and 40 $\text{ml}\cdot\text{min}^{-1}$ respectively. Throughout the process, the conductivity of the FS that
205 was recirculated in a closed loop system was monitored at room temperature with a

206 conductimeter (Hannah Instrument), as depicted in **Erreur! Source du renvoi**
 207 **introuvable.**(b). To mention that no significant water transmembrane migration was observed
 208 during the desalination experiments.



209
 210 **Figure 2:** (a) FCDI cell. (b) Experimental set-up and operating principle. CEM: cationic exchange
 211 membrane; AEM: anionic exchange membrane

212
 213 FCDI desalinating performance indicators were calculated for each experiment.

214 Salt adsorption capacity (SAC) indicating the mass of adsorbed salt as function of the
 215 adsorbent electrode weight is calculated according to equation (1) and expressed in mg of salt
 216 adsorbed per g of electrode material:

$$217 \quad SAC = \frac{(C_0 - C_f) V}{m_{electrode}} \quad (1)$$

218 Where C_0 is the initial solute concentration of the feed solution, C_f the final solute concentration,
 219 V is the volume of the feed solution and $m_{electrode}$ is the mass of the electrode material.²⁹

220
 221 The salt removal efficiency or desalination efficiency (DE) was calculated using equation (2):

$$223 \quad DE = \frac{(C_0 - C_f)}{C_0} \quad (2)$$

224
 225 where C_0 and C_f are the initial and final concentrations (mol. L⁻¹) of the FS.¹

226 The salt adsorption rate (SAR), which represents the amount of salt adsorbed (μg) per
 227 electrode surface (cm²) per unit of time (min), was calculated using equation (3):

228 $SAR (\mu\text{g} \cdot \text{cm}^{-2} \cdot \text{min}^{-1}) = \frac{(C_0 - C_f) V}{A t}$ (3)

229

230 where V is the volume of the feed solution (L), A is the contact area between the feed electrode
 231 and the current collector, and t is the charging time.³⁰

232 The charge efficiency (CE) or faradaic efficiency is the ratio of the electrical charges related
 233 specifically to ion removal over the total electrical charge applied by the potentiostat. It
 234 represents the energy efficiency of the system and was calculated using equation (4):

235

236 $CE = \frac{z (C_0 - C_f) V F}{\int I dt}$ (4)

237

238 where z is the equivalent charge of ions, V is the FS volume, F is the Faradaic constant, and
 239 $\int I dt$ is the integrated quantity of charge passed to the system over time.³¹

240 The Reynolds number shows the electrode flowing nature in the channel and was calculated
 241 with equation (5):

242 $Re = \frac{\rho v D}{\eta}$ (5)

243 where ρ and v are the flowable electrode density and velocity, respectively, in the flow channel
 244 calculated from the flow rate of the flowable electrode ($0.0024 \text{ m}^3 \text{ h}^{-1}$) to the area of the flow
 245 cell ($5.4 \times 10^{-6} \text{ m}^2$), D is the hydraulic diameter of the flow channel (6 mm), and η is the mean
 246 coefficient of dynamic viscosity of the flowable electrode in function of the shear rate at 25°C .

247 Stokes's law of sedimentation shows the drag force resisting the fall of small particles through
 248 a fluid medium under the influence of gravity, and is described by equation (6):

249 $V = \frac{2 (\rho_p - \rho_f) g R^2}{9 \eta}$ (6)

250 where ρ_p is the particle density, ρ_f is the fluid density, g is the acceleration of gravity, R is the
 251 particle radius, and η is the viscosity.³²

252 The linear pressure drop is the loss of mechanical energy caused by friction on the common
 253 walls of the network. It is directly affected by the fluid viscosity, and is described by equation
 254 (7):

255
$$\Delta P = \mu \frac{L}{D} \frac{1}{2} \rho v^2 \quad (7)$$

256 where μ is the friction coefficient with $\mu = 64/Re$, L and D are the canal length and diameter,
 257 ρ is the fluid apparent density, and v its velocity.³³

258 The electrical double-layer capacitance (EDLC) was calculated according to equation (8):

259
$$C_{EDL} = \frac{\int I dV}{2 u A \Delta V} \quad (8)$$

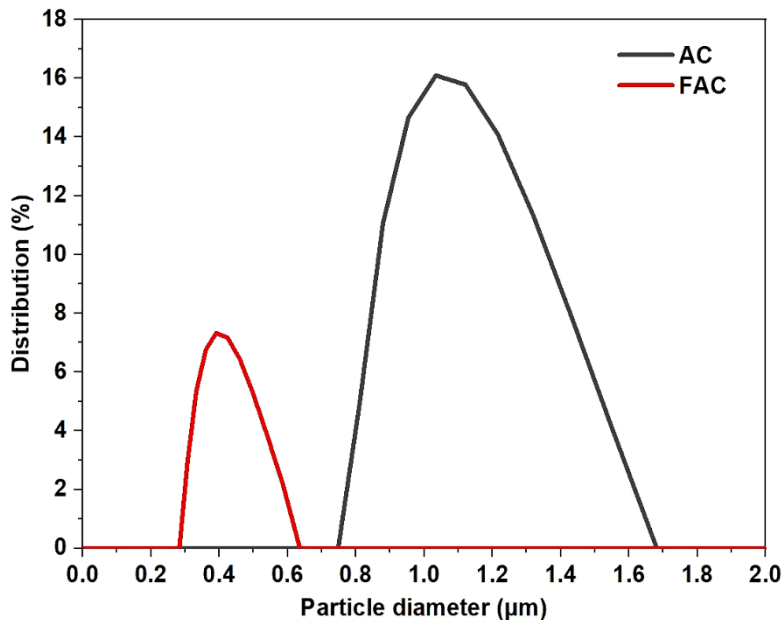
260 where C_{EDL} is the double layer capacitance, I is the current response, ΔV is the potential
 261 window, A is the effective area, and u is the scan rate.³⁴

262

263 3. Results and discussion

264 3.1. Particle size reduction

265 AC and FAC morphological and structural properties were investigated in our previous study.²⁸
 266 The dynamic light scattering (DLS) data (**Erreur ! Source du renvoi introuvable.** (a)) showed
 267 the difference in particle size distribution between pristine AC and FAC samples: 0.8-1.6 μm
 268 versus 0.3 to 0.6 μm respectively.



269 **Figure 3:** particle size distribution of AC and FAC after ball-milling measured by DLS method
 270

271

272 3.2. Structural and textural characteristics

273 The structural and textural characteristics as well as the chemical moieties and composition of
 274 AC and FAC samples were described in our previous study and are summarized in Figure S1,

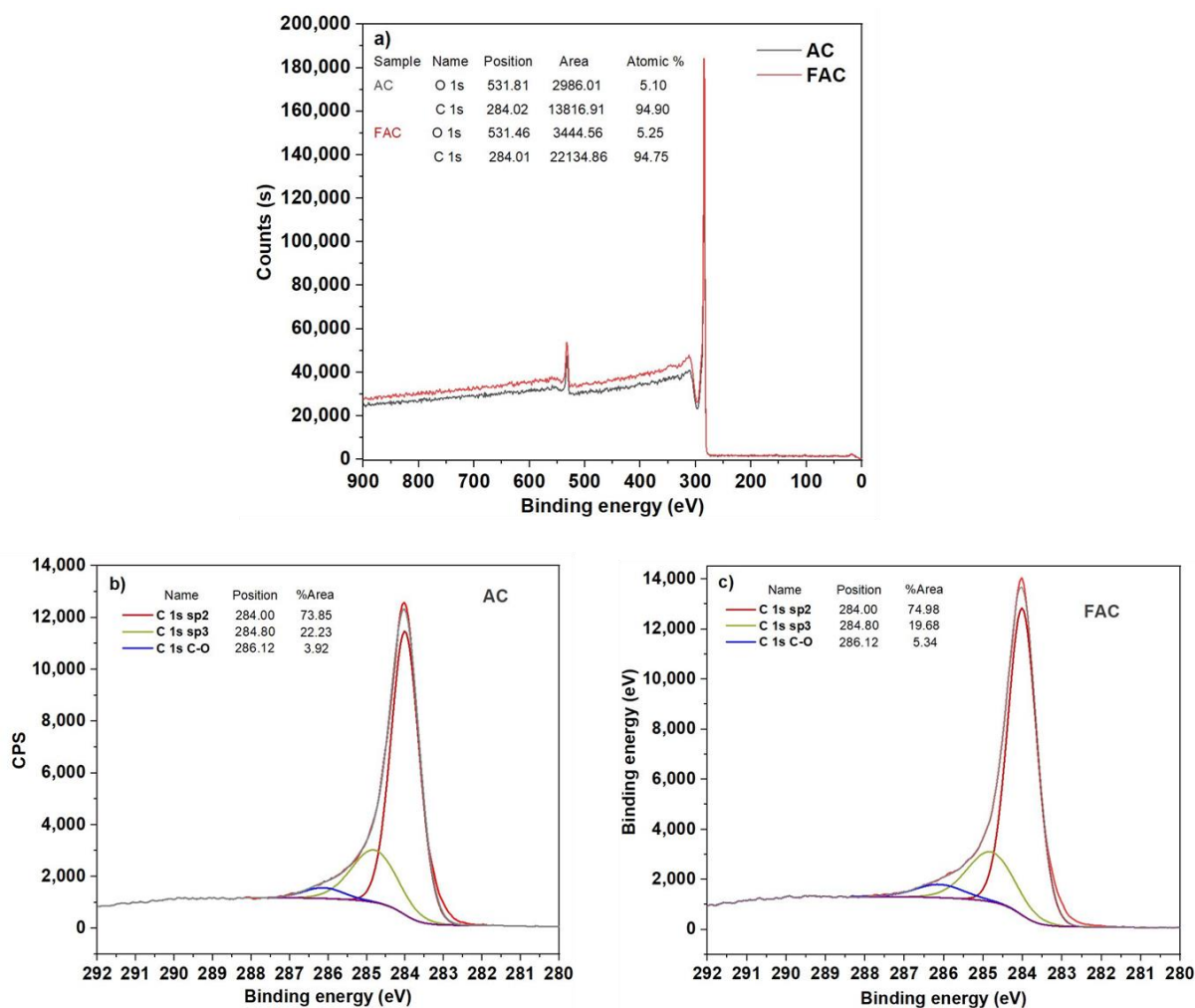
275 Table S1 and Figure S2 in supplementary information. Briefly, all AC characteristics were
276 maintained in FAC after dry ball grinding, without any significant difference in texture (pores
277 structure and surface area).²⁸

278

279 **3.3. Physical and chemical properties**

280 **3.3.1. Atomic composition**

281 The atomic composition of the carbon material before and after ball milling was investigated
282 using XPS. No band reduction was observed after ball milling. However, according to XPS
283 analysis, the O1s atomic percentage of the carbon material slightly increased after ball milling
284 from 5.10 % (AC) to 5.25 % (FAC), which can be due to the generation of new oxygenated
285 surface functional groups after ball milling. Figure 4 a shows the complete spectra of both AC
286 and FAC, while c and d present the resolved C 1s spectrum of AC and FAC respectively into
287 their individual peaks. 284.00, 284.80 and 286.10 eV binding energies correspond to C 1s sp²,
288 C 1s sp³ and C 1s C-O respectively.³⁵ As well Figure 4 b and c show a slight increase in the
289 C 1s C-O band area from 3.92% to 5.34% after ball milling (FAC) proving the formation of new
290 C-O functional groups on the surface of the activated carbon material.



291

292 **Figure 4:** XPS complete survey of AC and FAC (a), deconvoluted XPS C 1s spectra of AC (b) and
 293 FAC (c)

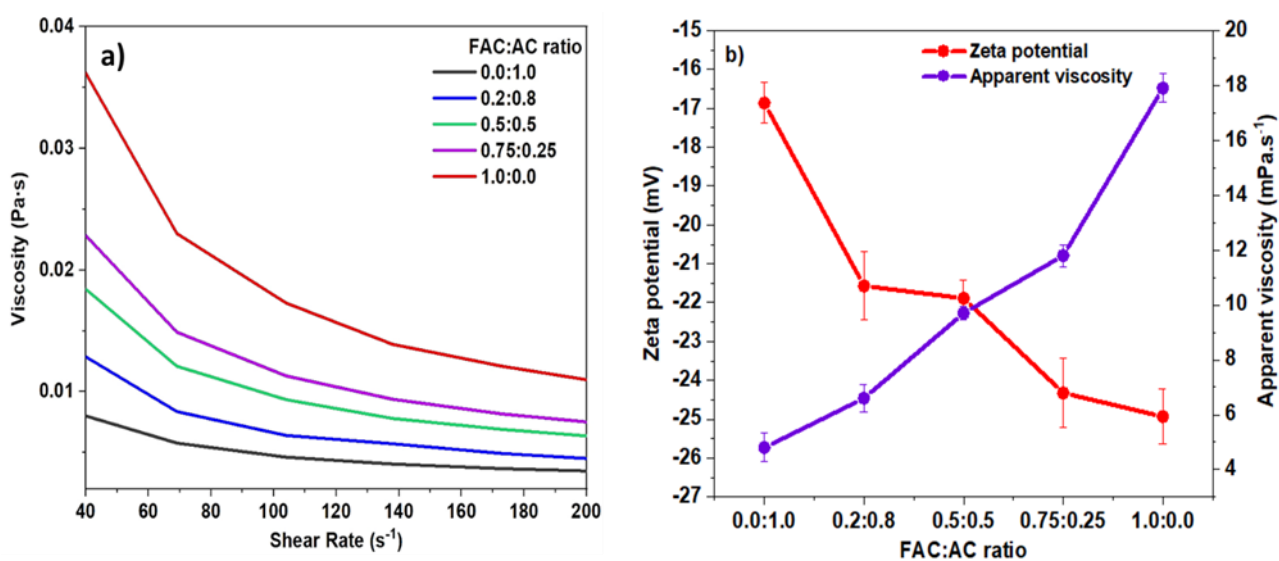
294

295 **3.3.2. Rheological properties and zeta potential: effect of particle distribution**

296 To improve the flowing properties of carbon-based flowable electrodes in FCDI systems,
 297 bimodal distributions were used by mixing (different ratios) of FAC (size range: 0.3-0.6 μm)
 298 and AC (size range: 0.8-1.6 μm). This was based on the hypothesis that fine particles can fill
 299 the gaps between larger particles (packing effect), increasing the connectivity within the carbon
 300 network, while keeping enough free spaces for water to flow through (i.e. acceptable viscosity).
 301 The packing effect on the dynamic viscosity and surface charge (zeta potential) was studied
 302 first by measuring the viscosity in function of the shear rate and zeta potential of carbon
 303 suspensions with monomodal and bimodal distributions (different FAC to AC ratios) (Figure).
 304 The apparent viscosities of all carbon suspensions decreased when the applied shear rate
 305 was increased, showing a flow behavior typical of a pseudo-plastic fluid, this phenomenon is
 306 typical of non-Newtonian fluids.³⁶ Moreover, their viscosity (Figure 5(a)) increased
 307 proportionally with the FAC percentage. Upon dry ball grinding of AC, each particle is divided
 308 into many particles, thus increasing the particle number for the same weight percentage and
 309 flowable electrode volume. Consequently, the higher specific surface area of particles
 310 increases interactions with water, and dissipates more energy due to friction. This also

311 promotes particle-particle interactions, notably repulsion forces, leading to higher resistance to
 312 flow or higher viscosity. This is observed particularly at low shear rates.³⁷ This effect becomes
 313 less significant at higher shear rates because the interactive forces between particles are less
 314 effective. Moreover, wide and narrow particle size ranges are associated with low and high
 315 viscosity, respectively.³⁸ This explains the lower viscosity of AC samples because their particle
 316 size range was wider than that of FAC samples. Suspensions with wide particle size
 317 distribution (large polydispersity) aggregate more easily than suspensions with narrow
 318 polydispersity. This gives more of free space that facilitates the movement (flow) of individual
 319 particles, and thus lower viscosity. These results are in agreement with those by Harmadi *et*
 320 *al.*³⁹ and Buranasrisak *et al.*⁴⁰ who studied the particle size effect on the rheology and stability
 321 of carbon-water mixtures.

322 Zeta potentials represent the surface charge of particles in suspension. The particle size
 323 effects on zeta potential and apparent viscosity was studied. The electrostatic repulsive forces
 324 of particles in suspension under an applied voltage depend on their surface charge. It was
 325 found that zeta potential increases after ball-milling, which can be attributed to the increase in
 326 oxygenated functional groups on the surface of the material as shown previously in the XPS
 327 study. The addition of large particles with low zeta potential to the flow electrodes leads to
 328 decreased repulsive behavior, and decrease the suspension viscosity because the smaller
 329 specific surface area leads to less friction, as explained previously. However, suspensions of
 330 finer particles, which have strong surface charge (high zeta potential) increase particle-particle
 331 repulsion and the resistance to flow or viscosity. Similarly, zeta potential measurements
 332 (Figure (b)) showed the interdependence between viscosity, surface charge, and FAC
 333 percentage. As finer particles in suspension have stronger surface charge (higher zeta
 334 potential), particle-particle repulsion is promoted, decreasing aggregation. Consequently, the
 335 whole space is occupied by well-dispersed particles, and less space is available for free water
 336 flow, leading to higher viscosity. Upon reducing FAC percentage in the suspension, repulsion
 337 forces between particles were decreased as well as resistance to flow, and therefore, flowing
 338 behavior in the FCDI system was improved. These results are fully in line with those by
 339 Buranasrisak *et al.*⁴⁰.



340
 341 **Figure 5:** (a) Viscosity of carbon suspensions with different FAC to AC ratios at different shear rates.
 342 (b) Dependence of the apparent viscosity on zeta potential and fine particle (FAC) fraction (100rps

343 shear rate). All experiments were carried out with carbon suspensions with 10 % wt carbon loading,
344 fine particle size range of 0.3-0.6 μm , and large particle size range of 0.8-1.6 μm .

345 **3.3.3. Reynolds number**

346 Reynolds number (i.e. the inertial forces to viscous forces ratio) is used to categorize the fluid
347 systems where viscosity has an important effect in controlling the fluid velocity or flow pattern,
348 a critical parameter in our study. For all mixtures, the Reynolds number (calculated using
349 equation (5)) was <2100, indicating a laminar flow (i.e. the flow type needed for flowable
350 electrodes in FCDI systems) (Table 2). As flow velocity is directly proportional to the Reynolds
351 number, this explains the decrease of the Reynolds number in carbon suspensions with higher
352 FAC percentages because they decrease the flow velocity. Consequently, when the viscosity
353 increased with higher FAC: AC ratios, the Reynolds number decreased.

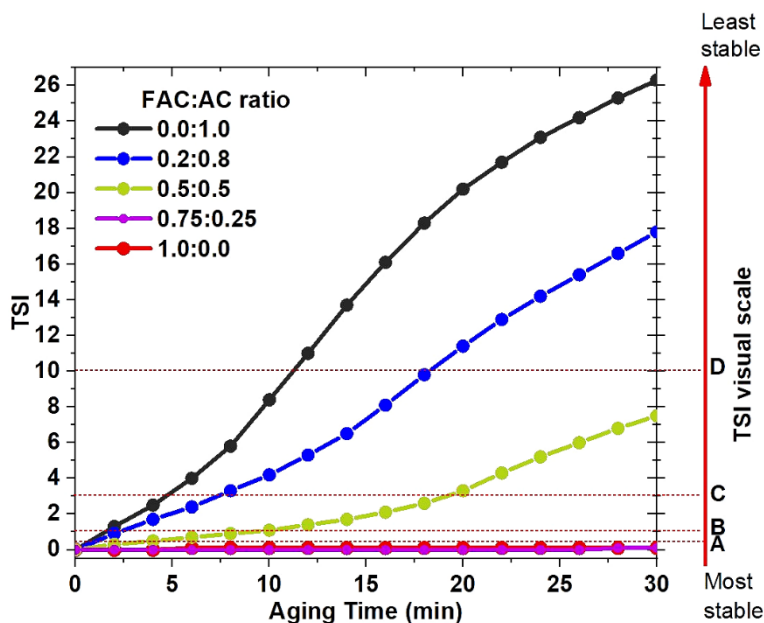
354 **Table 2:** Reynolds number of the indicated carbon suspensions

FAC : AC ratio	Reynolds n°
0.0 : 1.0	57.787 \pm 0.006
0.2 : 0.8	45.033 \pm 0.006
0.5 : 0.5	30.620 \pm 0.001
0.75 : 0.25	21.808 \pm 0.008
1.0 : 0.0	13.106 \pm 0.030

355

356 **3.3.4. Physical stability**

357 AC particles suspended in water tend to settle due to gravitational force. In FCDI systems, this
358 can cause clogging inside the channels, thus reducing the particle availability for ion adsorption
359 during the process. The destabilization kinetics of suspensions with different fine to large
360 particle ratios (at 10% wt) were evaluated by measuring the TSI (TURBISCAN® technology)
361 over 30 minutes (**Erreur ! Source du renvoi introuvable.**). The TSI (i.e. destabilization)
362 progressively increased for samples with lower FAC percentages. This indicates that the
363 stability of the carbon suspensions increased with higher FAC percentages, although no
364 difference was observed for samples with fine particles to large particle ratios of 0.75:0.25 and
365 1.0:0.0. Particle size reduction is associated with slower sedimentation rates. This is explained
366 by the sedimentation velocity law shown in equation (6). Indeed, the particle size has an effect
367 on the sedimentation velocity. According to Stokes' law, the particle sedimentation velocity is
368 proportional to the density difference between the solid and liquid phase, inversely proportional
369 to the fluid viscosity, and proportional to the particle diameter square. This explains the
370 important decrease in sedimentation velocity with FAC percentage increase in the
371 suspensions: smaller particle size is associated with higher viscosity. FAC particles remained
372 in suspension and well dispersed for a longer period of time, thus increasing the intra-particle
373 interactions in solution. These results are in agreement with the rheology and zeta potential
374 data, and explain the behavior of the different carbon particle size suspensions as flowable
375 electrodes.

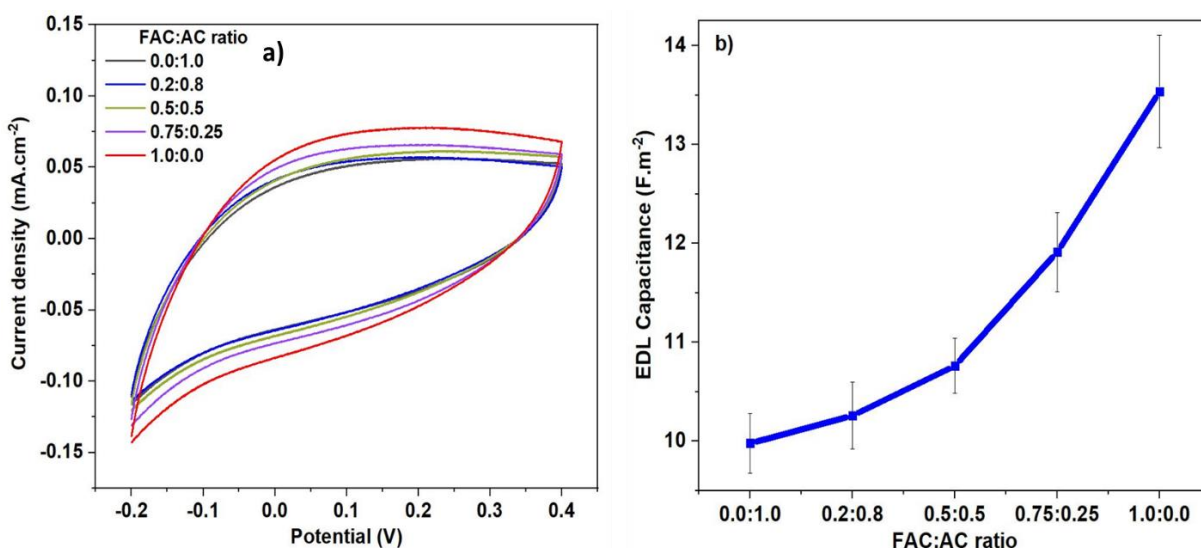


376

377 **Figure 6:** TURBISCAN® stability index (TSI) of the carbon suspensions at different ratios of fine particles
 378 to large particles. Below level A (lowest TSI dash line) on the TSI visual scale, no destabilization is
 379 observed. Level A marks the beginning of the very early destabilization stage. Level B indicates the
 380 beginning of destabilization, and levels C and D describe high sedimentation stages.

381 3.4. Electrochemical properties

382 To evaluate the electrochemical behavior of activated carbon electrodes with different
 383 FAC:AC ratios, cyclic voltammetry (CV) measurements were carried out using a 1 g/L NaCl
 384 electrolyte solution at 2 mV. s⁻¹ scan rate with a -0.2 – 0.4 V voltage window. The CV results
 385 are shown in Figure 7 (a). All the electrodes displayed a symmetrical box-like shape, which
 386 reflects good capacitor characteristic. The larger area obtained under the CV curves implies
 387 the higher specific capacitance of the materials. The 1.0: 0.0 FAC: AC ratio (pure FAC)
 388 electrode showed the highest area obtained under the CV curves, indicating the highest
 389 specific capacitance compared to the pure AC electrode. As well, based on the cyclic
 390 voltammetry cycles, the EDL capacitance of the different electrodes of different FAC: AC
 391 ratios was calculated according to equation 8 and presented in figure 7 (b).⁴¹ Thus, in all
 392 cases, the addition of FAC to the AC electrodes enhances their double layer capacitance due
 393 to the increased conductivity of the flow electrodes caused by the improved interconnectivity
 394 between the carbon particles in the case of FAC as explained in details before. Thus pure
 395 FAC electrode showed the highest specific capacitance of 35 F.cm⁻² compared to 25.5 F.cm⁻²
 396 in the case of pure AC marking a higher conductivity of FAC compared to AC.



397

398 **Figure 7:** Cyclic voltammety cycles (a) and electrical double layer capacitance (b) for activated
399 carbon electrodes with different FAC:AC ratios.

400 3.5. Desalination performance

401 The electrosorption characteristics of the different carbon suspensions (10% wt carbon
402 loading) as flow electrodes were investigated without clogging in our FCDI set-up. FCDI
403 performance indicators (DE, SAC, SAR and CE) were calculated for the different mixtures
404 (Table 3 and Figure (b and c)). In all cases, FAC addition strongly improved their salt adsorption
405 capacity and desalination performance in FCDI. The higher specific surface area, more
406 accessible pores, better conductivity observed upon particle size reduction explain the
407 improved DE, SAC, and SAR values (Table 3, Figure 8 (b)). Higher surface area promotes
408 mass transfer (ion adsorption), which is the limiting mass transfer phenomenon in FCDI. This
409 strongly influences the SAR values, as seen after FAC addition in the flowable electrodes.

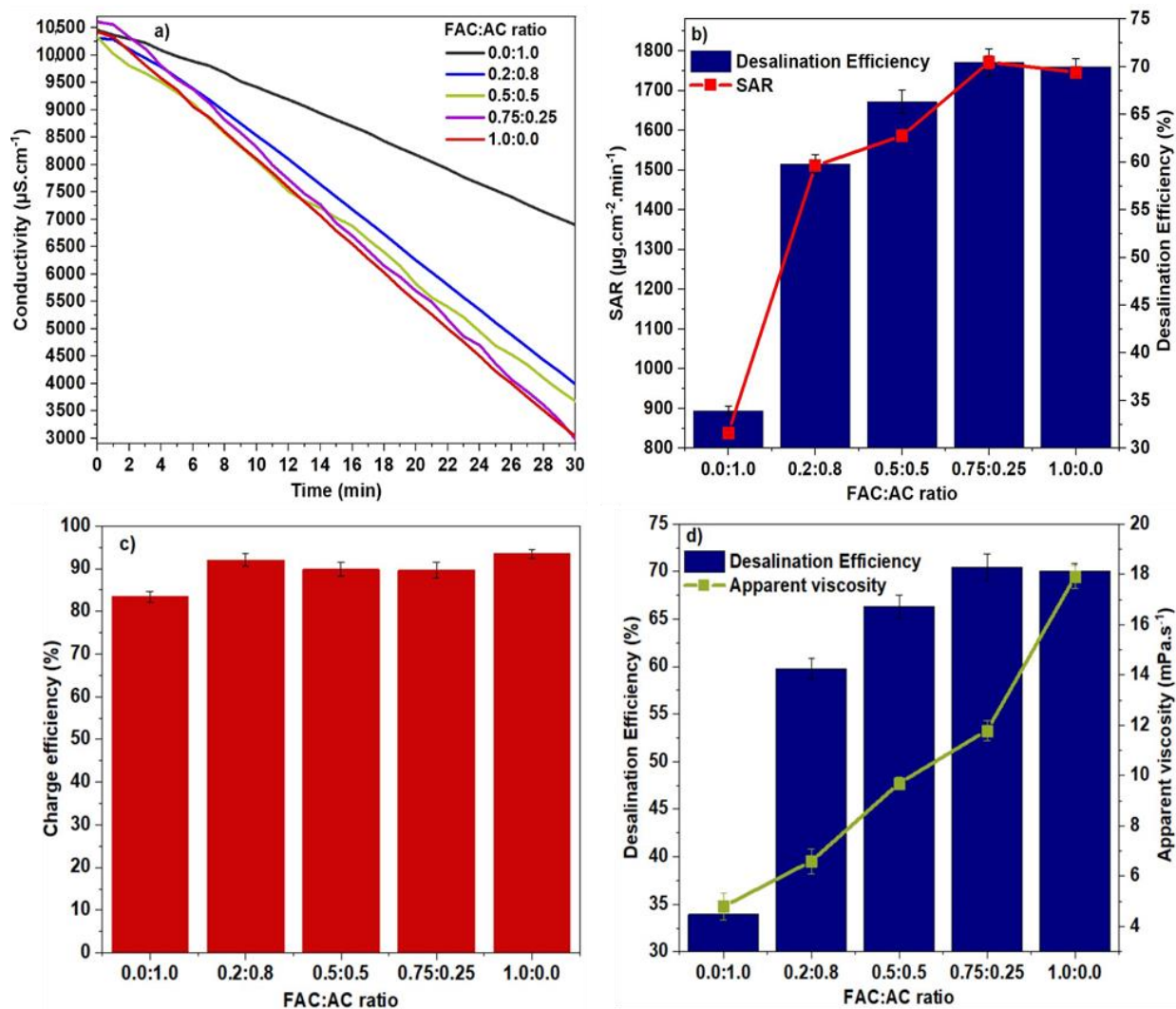
410 Sharper drop in ionic conductivity of the FS when using bimodal mixtures or pure FAC
411 compared with pure AC was observed (Figure 7 (a)). Flowable electrodes with 0.75:0.25 and
412 1.0:0.0 FAC:AC ratios exhibited the best DE, the highest SAC and SAR among all samples
413 (Table 3 Figure 8 (b and c)). DE was 72%, SAC was 32.3 mg.g⁻¹, and SAR was 1772 μg.cm⁻².min⁻¹
414 for the 0.75:0.25 sample compared with 34%, 15.3 mg.g⁻¹ and 839 μg.cm⁻².min⁻¹ for the
415 pure AC flow electrode respectively. This can be due to the improved ion diffusion pathways
416 within the carbon network because fine particles filled the void between larger particles, thus
417 increasing contact areas within the carbon network, and consequently conductivity in the
418 flowable electrode. The lower desalination performance of the flowable electrode with AC
419 particles might be due to the lower repulsion forces between particles that aggregate to each
420 other, thus masking the pores that become less accessible to ions. Furthermore, the higher
421 resistance and lower conductivity caused by water occupying the large gaps between large
422 AC particles create long ion diffusion pathways. These parameters explain the lower
423 performance metrics of these flowable electrodes. The chronoamperometry curves (Figure S3
424 in SI) for the different carbon slurries showed the current density in function of time at a
425 constant applied voltage (1V). Current density was lower for pure AC suspensions than for the
426 samples with different FAC percentages. Therefore, the total charge transferred (which is the
427 integration of the chronoamperometry curves) was lower for large AC particles, resulting in
428 lower DE. The current density progressively increased with the percentage of FAC added, and

429 DE improved. Conversely, CE was comparable among samples (Figure 8 (c)), likely because
 430 this parameter is mostly influenced by the ion transfer through the selective IEM. For all
 431 samples, the same FCDI system with the same IEM was used, the conductivity of the saline
 432 solution passing between the electrodes was the same (5 g/L NaCl), and the quantity of carbon
 433 in the electrode compartments was largely enough to receive ions from the central
 434 compartment. The high selectivity of cationic and anionic membranes in such conditions
 435 explains the comparable CE values among samples.⁴² Analysis of the relationship between
 436 the apparent viscosity and DE of the different flowable electrodes (Figure 8 (d)) showed that
 437 with the 0.75:0.25 FAC:AC ratio bimodal mixture, viscosity decreased by 30%, overcoming the
 438 major limitation of FAC-based flowable electrodes in FCDI (i.e. high viscosity). The challenge
 439 is always to find a compromise between these parameters to improve desalination
 440 performance in FCDI, while maintaining good flowing properties of the electrodes inside the
 441 system. In this study a good compromise between these parameters was achieved with the
 442 0.75:0.25 FAC:AC ratio bimodal mixture.

443 **Table 3:** salt adsorption capacity (SAC) and average salt adsorption rate (SAR) of carbon flow
 444 electrodes with different FAC : AC ratio

FAC : AC ratio	SAC (mg.g⁻¹)	SAR (µg.cm⁻².min⁻¹)
0.0 : 1.0	15.3	0.51
0.2 : 0.8	27.6	0.92
0.5 : 0.5	28.9	0.96
0.75 : 0.25	32.3	1.08
1.0 : 0.0	31.9	1.06

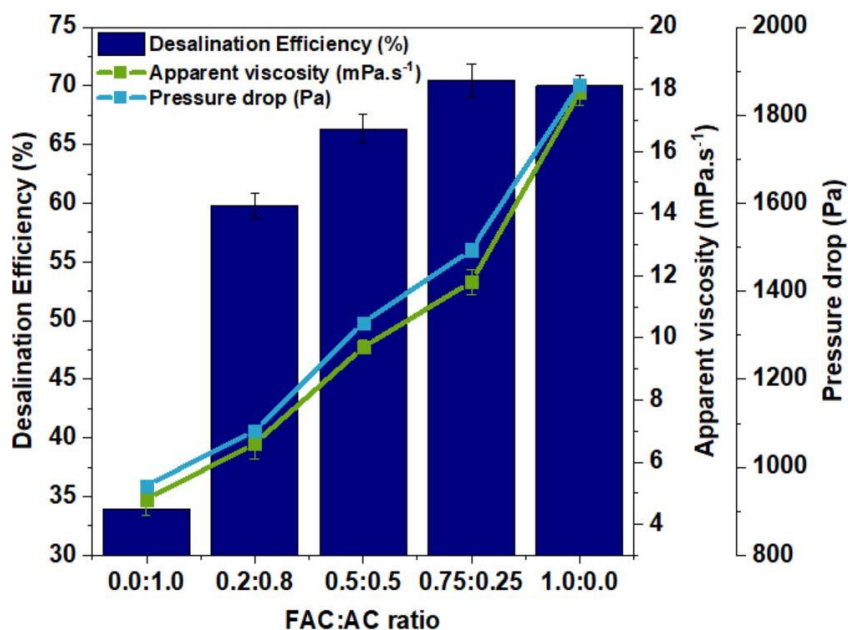
445



446

447 **Figure 8:** Feed solution conductivity (a), desalination efficiency and salt adsorption rate (SAR) (b), and
 448 charge efficiency (c) of carbon-based flowable electrodes with different FAC: AC ratios, during 30 min of
 FCDI experiment time. Relationship between desalination efficiency and apparent viscosity (d).

449 The rheological characteristics of the carbon slurries were studied to optimize their flowability
 450 inside the FCDI system because this has a direct effect on the pumping energy and cost. To
 451 this aim, viscosity effect on the pressure drop was assessed when comparing the desalination
 452 performances of the different flowable electrodes. In every FCDI process, there is always a
 453 compromise between particle size and viscosity. Smaller carbon particles increase
 454 conductivity, and consequently the process efficiency, for instance in terms of charge transfer,
 455 maximum salt capacity, mass transfer. However, adding small particles to the carbon slurry
 456 increases viscosity and also pumping costs due to the pressure drop increase. In our set-up,
 457 pressure drop (calculated with equation (7)) increased with the viscosity increase (Figure 9).
 458 With higher FAC percentages in the slurry, DE improved but viscosity increased, and also the
 459 pressure drop, leading to higher pumping energy and costs. Therefore, it is important to find
 460 the best compromise between particle size distribution and viscosity in order to obtain an
 461 energy-efficient process with good performance without clogging problems inside the FCDI
 462 system.



463

464 **Figure 9:** Relationship between desalination efficiency, apparent viscosity, and pressure drop increase
 465 of carbon-based flowable electrodes with the indicated FAC: AC ratios, during 30 min of FCDI
 466 experiment time.

467

468 **4. Conclusion**

469 This work investigated the effect of particle size distribution on the viscosity and desalination
 470 performance of AC-based flowable electrodes in FCDI. Mixtures of two different AC particle
 471 sizes were used: commercial AC and FAC obtained after ball-milling commercial AC. This
 472 experimental work shows that particle size distribution has a considerable effect on ion
 473 diffusion length and on the ion transport pathway that is determined by the packing density of
 474 flowable electrodes. Particularly, with pure AC suspensions, intraparticle and interparticle ion
 475 diffusion limited the desalination capacity (34% of DE). By mixing two different particle sizes,
 476 particle size distribution became broader, leading to better desalination performance, as
 477 indicated by the 72% of DE and improved flowing properties of the flowable electrode in FCDI
 478 (decrease by 33% of viscosity compared with the pure FAC suspension that achieved 70% of
 479 DE) in FCDI. These results highlighted the importance of particle size distribution and packing
 480 density on the behavior of flowable electrodes optimized for FCDI-based desalination. Fine
 481 particles and combined (0.75: 0.25 FAC: AC ratio) slurries showed better desalination
 482 performance compared to large particle slurries. However, large particle slurries showed better
 483 fluidity and easier flow in our water desalination system leading to lower pressure drop. Thus,
 484 good compromise must be done between high desalination capacity and acceptable pressure
 485 drop (viscosity) to have an optimal electrochemical desalination process. To find the best
 486 balance, more research is needed, including molecular dynamic simulations that can improve
 487 experimental procedures and save time.

488

489 **Author Contributions:** Conceptualization: M.T.; Methodology: M.B and M.C.; Formal
 490 analysis: M.T. S.L. and M.B. Investigation: M.T.; Resources: F.Z., M.B., P.S. and M.C.; Data

491 curation: M.T.; Original draft preparation: M.T.; Writing, review and editing: M.T., F.Z., M.B.
492 and M.C.; Visualization: F.Z., M.T., M.B. and M.C.; Supervision: F.Z., M.B., P.S. and M.C.;
493 Project administration: M.B., F.Z., P.S. and M.C. All authors have read and agreed to the
494 published version of the manuscript.

495

496

497 **Conflicts of Interest:** The authors declare no conflict of interest.

498

499 **References**

- 500 1. Folaranmi, G. *et al.* Towards Electrochemical Water Desalination Techniques: A Review on
501 Capacitive Deionization, Membrane Capacitive Deionization and Flow Capacitive Deionization.
502 *Membranes* **10**, E96 (2020).
- 503 2. Jeon, S. *et al.* Desalination via a new membrane capacitive deionization process utilizing flow-
504 electrodes. *Energy Environ. Sci.* **6**, 1471–1475 (2013).
- 505 3. Seo, S.-J. *et al.* Investigation on removal of hardness ions by capacitive deionization (CDI) for
506 water softening applications. *Water Res.* **44**, 2267–2275 (2010).
- 507 4. Kalfa, A. *et al.* Capacitive deionization for wastewater treatment: Opportunities and challenges.
508 *Chemosphere* **241**, 125003 (2020).
- 509 5. Porada, S. *et al.* Review on the science and technology of water desalination by capacitive
510 deionization. *Prog. Mater. Sci.* **58**, 1388–1442 (2013).
- 511 6. Lee, J.-B. *et al.* Desalination of a thermal power plant wastewater by membrane capacitive
512 deionization. *Desalination* **196**, 125–134 (2006).
- 513 7. Andelman, M. D. *et al.* Charge barrier flow-through capacitor. (2004).
- 514 8. Biesheuvel, P. M. *et al.* Theory of membrane capacitive deionization including the effect of the
515 electrode pore space. *J. Colloid Interface Sci.* **360**, 239–248 (2011).

- 516 9. Zhang, C. *et al.* Flow Electrode Capacitive Deionization (FCDI): Recent Developments,
517 Environmental Applications, and Future Perspectives. *Environ. Sci. Technol.* **55**, 4243–4267
518 (2021).
- 519 10. Presser, V. *et al.* The Electrochemical Flow Capacitor: A New Concept for Rapid Energy Storage
520 and Recovery. *Adv. Energy Mater.* **2**, 895–902 (2012).
- 521 11. Tang, K. *et al.* Optimal conditions for efficient flow-electrode capacitive deionization. *Sep. Purif.*
522 *Technol.* **240**, 116626 (2020).
- 523 12. Liu, Z. *et al.* A Brief Review on High-Performance Capacitive Deionization Enabled by
524 Intercalation Electrodes. *Glob. Chall.* **5**, 2000054 (2021).
- 525 13. Ma, J. *et al.* Flow-electrode capacitive deionization (FCDI) scale-up using a membrane stack
526 configuration. *Water Res.* **168**, 115186 (2020).
- 527 14. Tang, K. *et al.* Water Desalination by Flow-Electrode Capacitive Deionization in Overlimiting
528 Current Regimes. *Environ. Sci. Technol.* **54**, 5853–5863 (2020).
- 529 15. Shi, W. *et al.* Exploration of Energy Storage Materials for Water Desalination via Next-Generation
530 Capacitive Deionization. *Front. Chem.* **8**, 415 (2020).
- 531 16. Ryoo, M.-W. *et al.* Improvement in capacitive deionization function of activated carbon cloth by
532 titania modification. *Water Res.* **37**, 1527–1534 (2003).
- 533 17. Hou, C.-H. *et al.* Development of multi-walled carbon nanotube/poly(vinyl alcohol) composite as
534 electrode for capacitive deionization. *Sep. Purif. Technol.* **130**, 7–14 (2014).
- 535 18. El-Deen, A. *et al.* Graphene wrapped MnO₂-nanostructures as effective and stable electrode
536 materials for capacitive deionization desalination technology. *Desalination* **344**, 289–298 (2014).
- 537 19. Liu, X. *et al.* Fabrication of graphene/activated carbon nanofiber composites for high
538 performance capacitive deionization. *J. Taiwan Inst. Chem. Eng.* **72**, 213–219 (2017).
- 539 20. Park, K.-K. *et al.* Development of a carbon sheet electrode for electrosorption desalination.
540 *Desalination* **206**, 86–91 (2007).

- 541 21. Cheng, Y. *et al.* A review of modification of carbon electrode material in capacitive deionization.
542 *RSC Adv.* **9**, 24401–24419 (2019).
- 543 22. Zhao, X. *et al.* Electrode materials for capacitive deionization: A review. *J. Electroanal. Chem.*
544 **873**, 114416 (2020).
- 545 23. Huang, K. *et al.* Significantly increasing porosity of mesoporous carbon by NaNH₂ activation for
546 enhanced CO₂ adsorption. *Microporous Mesoporous Mater.* **230**, (2016).
- 547 24. Teng, H. *et al.* High-Porosity Carbons Prepared from Bituminous Coal with Potassium Hydroxide
548 Activation. *Ind. Eng. Chem. Res.* **38**, 2947–2953 (1999).
- 549 25. Zhang, H. *et al.* Constructing Hierarchical Porous Carbons With Interconnected Micro-mesopores
550 for Enhanced CO₂ Adsorption. *Front. Chem.* **7**, (2020).
- 551 26. Zhang, Y. *et al.* Particle size distribution influence on capacitive deionization: Insights for
552 electrode preparation. *Desalination* **525**, 115503 (2022).
- 553 27. Cohen, H. *et al.* E. Suspension Electrodes Combining Slurries and Upflow Fluidized Beds.
554 *ChemSusChem* **9**, 3045–3048 (2016).
- 555 28. Folaranmi, G. *et al.* Investigation of fine activated carbon as a viable flow electrode in capacitive
556 deionization. *Desalination* **525**, 115500 (2022).
- 557 29. Jung, Y. *et al.* Enhanced Electrochemical Stability of a Zwitterionic-Polymer-Functionalized
558 Electrode for Capacitive Deionization. *ACS Appl. Mater. Interfaces* **10**, 6207–6217 (2018).
- 559 30. Zhao, R. *et al.* Optimization of salt adsorption rate in membrane capacitive deionization. *Water*
560 *Res.* **47**, 1941–1952 (2013).
- 561 31. Porada, S. *et al.* Direct prediction of the desalination performance of porous carbon electrodes
562 for capacitive deionization. *Energy Environ. Sci.* **6**, 3700–3712 (2013).
- 563 32. Bridges, S. *et al.* Chapter 1 - Rheology. in *A Practical Handbook for Drilling Fluids Processing* (eds.
564 Bridges, S. & Robinson, L.) 3–26 (Gulf Professional Publishing, 2020).

- 565 33. Meister, F. *et al.* 6 - Additional clinical applications. in *Artificial Intelligence for Computational*
566 *Modeling of the Heart* (eds. Mansi, T., Passerini, T. & Comaniciu, D.) 183–210 (Academic Press,
567 2020). doi:10.1016/B978-0-12-817594-1.00017-6.
- 568 34. Chandra, S. *et al.* Molecular Level Control of the Capacitance of Two-Dimensional Covalent
569 Organic Frameworks: Role of Hydrogen Bonding in Energy Storage Materials. *Chem. Mater.* **29**,
570 2074–2080 (2017).
- 571 35. Rossin, J. A. XPS surface studies of activated carbon. *Carbon* **27**, 611–613 (1989).
- 572 36. Poslinski, A. J. *et al.* Rheological Behavior of Filled Polymeric Systems I. Yield Stress and Shear-
573 Thinning Effects. *J. Rheol.* **32**, 703–735 (1988).
- 574 37. Hou, H. *et al.* Quantifying effects of particulate properties on powder flow properties using a ring
575 shear tester. *J. Pharm. Sci.* **97**, 4030–4039 (2008).
- 576 38. Barthelmes, G. *et al.* Particle size distributions and viscosity of suspensions undergoing shear-
577 induced coagulation and fragmentation. *Chem. Eng. Sci.* **58**, 2893–2902 (2003).
- 578 39. Harmadi, E. *et al.* Effect of Particle Size Distribution on Rheology and Stability of High
579 Concentration Coal-Water Mixture (Cwm) With Indonesian Low Rank Coal. *undefined* (2009).
- 580 40. Buranasrisak, P. *et al.* Effects of Particle Size Distribution and Packing Characteristics on the
581 Preparation of Highly-Loaded Coal-Water Slurry. *Int. J. Chem. Eng. Appl.* **3**, 31–35 (2012).
- 582 41. Jiménez, M. L. *et al.* Multiionic effects on the capacitance of porous electrodes. *Phys. Chem.*
583 *Chem. Phys.* **20**, 5012–5020 (2018).
- 584 42. Pismenskaya, N. *et al.* A Review on Ion-Exchange Membranes Fouling during Electrodialysis
585 Process in Food Industry, Part 2: Influence on Transport Properties and Electrochemical
586 Characteristics, Cleaning and Its Consequences. *Membranes* **11**, 811 (2021).
- 587
- 588
- 589